Langmuir

Article

pubs.acs.org/Langmuir

Docetaxel-Loaded Fluorescent Liquid-Crystalline Nanoparticles for Cancer Theranostics

Valeria Meli,[†] Claudia Caltagirone,*[,†] Angela M. Falchi,[‡] Stephen T. Hyde,[§] Vito Lippolis,[†] Maura Monduzzi,[†] Marc Obiols-Rabasa,[∥] Antonella Rosa,[‡] Judith Schmidt,[⊥] Yeshayahu Talmon,[⊥] and Sergio Murgia*[,†]

[†]Dipartimento di Scienze Chimiche e Geologiche and [‡]Dipartimento di Scienze Biomediche, Università degli Studi di Cagliari, S.S. 554 Bivio per Sestu, 09042 Monserrato, Italy

[§]Department of Applied Mathematics, Research School of Physics and Engineering, The Australian National University, Canberra, A.C.T. 0200, Australia

[∥]Division of Physical Chemistry, Department of Chemistry, Lund University, Getingevägen 60, SE-22240 Lund, Sweden

[⊥]Department of Chemical Engineering, Technion − Israel Institute of Technology, Haifa 3200003, Israel

ABSTRACT: Here, we describe a novel monoolein-based cubosome formulation engineered for possible theranostic applications in oncology. The Docetaxel-loaded nanoparticles were stabilized in water by a mixture of commercial Pluronic (poly(ethylene oxide)-poly(propylene oxide)-poly(ethylene oxide) triblock copolymer) F108 (PF108) and rhodamine- and folate-conjugated PF108 so that the nanoparticles possess targeting, therapeutic, and imaging properties. Nanoparticles were investigated by DLS, cryo-TEM, and SAXS to confirm their structural features. The fluorescent emission characterization of the proposed formulation indicated that the rhodamine conjugated to the PF108 experiences an environment less polar than water (similar to chloroform), suggesting that the fluorescent fragment is buried within the poly(ethylene oxide) corona surrounding the nanoparticle. Furthermore, these nanoparticles were successfully used to image living HeLa cells and demonstrated a significant short-term (4 h incubation) cytotoxicity effect against these cancer cells. Furthermore, given their analogy as nanocarriers for molecules of pharmaceutical interest and to better stress the singularities of these bicontinuous cubic nanoparticles, we also quantitatively evaluated the differences between cubosomes and multilamellar liposomes in terms of surface area and hydrophobic volume.

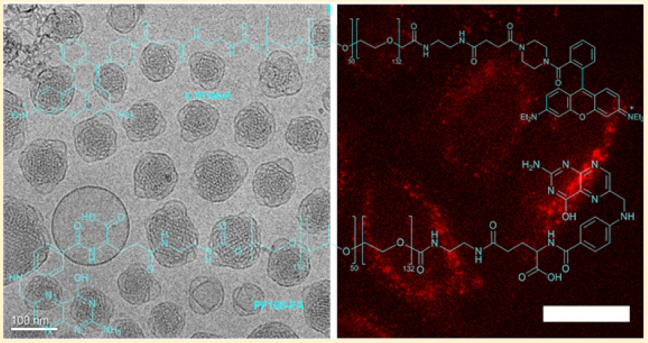

1. INTRODUCTION

The amphiphilic characteristics of polar lipids drive their self-assembly in water, giving a number of liquid-crystalline phases.[1,2] Among them, the most interesting are probably the reverse bicontinuous cubic phases.[3] These are a family of three-dimensional cubic structures constituted by a curved, non-intersecting lipid bilayer folded to form two disconnected, continuous water channels with a crystal lattice that can be described by three different types of infinite periodic minimal surfaces: the double diamond (space group $Pn\underline{3}m$), the gyroid (space group $Ia\underline{3}d$), and the primitive (space group $Im\underline{3}m$). These phases have been extensively investigated in recent decades because they represent versatile nanostructures able to incorporate molecules of biological relevance.[4−8] Interestingly, cubic phases can be formulated as aqueous nanoparticle dispersions, known as cubosomes.[9] Although various emulsifiers have been suggested,[10,11] in general, the stabilization in water of such liquid-crystalline nanoparticles is achieved using amphiphilic polymers having long poly(ethylene oxide) (PEO) chains, e.g., Pluronics (poly(ethylene oxide)-poly(propylene oxide)-poly(ethylene oxide) triblock copolymers) or polysorbate 80.[9,12]

Similar to the reverse liquid-crystalline cubic bulk phases, pharmaceutical applications are predicted for cubosomes,[13−17] and their potential use as nanocarriers for MRI probes has been investigated.[18,19] These nanoparticles have also been proposed for theranostic applications.[20−25] Indeed, several peculiar characteristics make cubosomes appealing as theranostic tools in oncology. Among these, one of the most distinguishing is the higher hydrophobic volume with respect to liposomes, often considered to be the golden standard for lipid-based nanocarriers in medicine. However, a quantitative comparison of the hydrophobic portion of these two kinds of nanoparticles has never been reported in the literature. Other cubosome-specific features are the simultaneous possibility of host therapeutics and imaging agents as well as a size (typically in the range 100−

Received: June 8, 2015
Revised: August 13, 2015
Published: August 20, 2015

ACS Publications © 2015 American Chemical Society

DOI: 10.1021/acs.langmuir.5b02101
Langmuir 2015, 31, 9566−9575

200 nm) that, at least in principle, allows the exploitation of the enhanced permeation retention mechanism for the passive targeting of cancer tissues.[9,26] In view of their application as nanomedicine, it is also worth mentioning that the clearance from the bloodstream via the mononuclear phagocytic system should be retarded since, by analogy to stealth liposomes, these nanoparticles are enclosed within a sort of a PEO corona that should prevent efficient recognition by opsonin, thus hindering phagocytosis.[27] Moreover, it was demonstrated that cubosomes (and hexosomes) can be suitably formulated by covering their surface with folate residues[20,28] or anti-EGFR Fab[29] to actively target these nanocarriers toward cancer cells, while the effects on the subcellular level of pristine monoolein-based cubosomes were recently investigated for HeLa cells.[30] Remarkably, nanoparticles with reverse bicontinuous cubic internal structure endowed with long-time stability and thermoresponsive capabilities can be formulated using polymer−surfactant mixtures.[31]

To explore further the potential of lipid-based liquid-crystalline nanoparticles as theranostic nanomedicine in cancer treatments, we report here the loading of monoolein-based cubosomes with a potent anticancer drug (Docetaxel). Such a formulation was stabilized with a mixture of commercial Pluronic F108 (PF108), folate-conjugated PF108 (PF108-FA), and rhodamine-conjugated PF108 (PF108-R) to simultaneously confer targeting, therapeutic, and imaging abilities on these nanoparticles. It deserves notice that engineering stable, multifunctional cubosome formulations can be a hard task. While the hydrophobic effect represents the main force that drives the self-assembly of the lipids constituting the nanoparticles, their inner phase is basically determined by the geometrical features of the lipid hydrophobic tail and polar head. This is rationalized by the molecular effective packing parameter (P_{eff}) given by the ratio v/al, where v and l are, respectively, the hydrophobic chain volume and length (taken as 80% of the fully extended chain) and a is the headgroup area.[1] P_{eff} is strongly dependent on the surrounding environment; therefore, the type of phase that characterizes the nanoparticles (and their very existence) is barely predictable in the presence of additives, since encapsulation within the lipid bilayer of molecules useful for giving these nanoparticles theranostic skills may significantly alter P_{eff}, thus provoking the transition of the inner phase or the collapse of the formulation.[9] In addition, the decoration of the cubosome surface with targeting and/or fluorescent moieties may disturb both the colloidal stability of the formulation and the cellular uptake of the nanoparticles. Throughout this paper we will demonstrate that the proposed cubosome formulation, although prepared with a high portion (40%) of conjugated PF108, is stable and successfully delivers its cargo to HeLa cells, taken as the standard for cancer cells.

Moreover, considering the analogies between liposomes and cubosomes, we also presented here a theoretical evaluation of the hydrophobic volume of these liquid-crystalline nanoparticles.

2. MATERIALS AND METHODS

2.1. Materials. Monoolein (MO, 1-monooleoylglycerol, RYLO MG 19 PHARMA, glycerol monooleate, 98.1 wt %) was kindly provided by Danisco A/S, DK-7200, Grinsted, Denmark. Pluronic F108 (PEO_{132}-PPO_{50}-PEO_{132}), Docetaxel (≥97%), *N*-hydroxysuccinimmide (NHS, 98%), *N*,*N*′-dicyclohexylcarbodiimide (DCC, ≥ 99.5%), triethylamine (≥99.5%), and dimethyl sulfoxide (≥99.7%) were purchased from Sigma-Aldrich. Distilled water passed through a Milli-Q water purification system (Millipore) was used to prepare the samples.

2.2. Sample Preparation. Monoolein-based cubosomes were prepared and stabilized by dispersing the appropriate amount of MO in aqueous solutions of a 60/20/20 mixture of Pluronic F108 (PF108) and folate-conjugated and rhodamine-conjugated PF108 (PF108/PF108-FA/PF108-R) using an ultrasonic processor (UP100H by Dr. Hielscher, cycle 0.9, amplitude 90%) for 10 min. Docetaxel-doped cubosomes were obtained by dispersing the drug in the melted lipids (at 37 °C) with the help of an ultrasonic bath before mixing with the Pluronic solution. The sample volume was usually 4 mL with approximately 96.4 wt % water, 3.3 wt % MO, and 0.3 wt % Pluronics mixture.

2.3. Synthesis of Rhodamine-Conjugated PF108 (PF108-R). PF108-NH_2 (0.1976 g, 0.013 mmol), *N*-hydroxysuccinimmide (NHS, 0.0125 g, 0.108 mmol), *N*,*N*′-dicyclohexylcarbodiimide (DCC, 0.0188 g, 0.091 mmol), and *N*-(9-(2-(4-(3-carboxypropanoyl)piperazine-1-carbonyl)benzyl)-6-(diethylamino)-3*H*-xanthen-3-ylidene)-*N*-ethylethanaminium (**4**; 0.024 g, 0.039 mmol) were dissolved in 8 mL of anhydrous DMSO in the presence of triethylamine (20 μL). To precipitate DCU (dicyclohexylurea), 20 mL of deionized water was added, and the mixture was then centrifuged and filtered to obtain a red limpid solution. This was dialyzed (14 kDa MW cutoff membrane) for 3 days against ultrapure water, which was changed every 2−6 h. The resulting product was lyophilized for 1 day to remove all of the residual water. Yield 63% (130.3 mg, 0.008 mmol); mp 48−50 °C. ^{1}H NMR (400 MHz, DMSO-d_6, 298 K): δH 1.045 (3H × 50, $-CH_3$ of PPO), 1.17−1.33 (m, 3H × 2, $-N(CH_2-\mathbf{CH_3})_2$), 2.66−2.69 (m, 4H × 2, aliphatic protons from rhodamine moiety), 3.29−3.55 (m, 3H × 50, 4H × 264, $-CH_2-CH(CH_3)-O-$ of PPO and $-CH_2-CH_2-O-$ of PEO), 3.60−3.73 (m, 2H × 2, $-N(\mathbf{CH_2}-CH_3)_2$), 4.53−4.56 (m, 1H × 2, amidic −NH), 6.95−8.07 (m, 10H × 2, aromatic protons). IR (solid state, cm^{-1}) ν = 2876 (s), 1584, 1635, 1714 (w).

2.4. Photophysical Characterization. Cubosome dispersions were diluted with Milli-Q water (1:100) before performing the photophysical measurements. The emission and excitation spectra were recorded with a PerkinElmer LS 55 spectrofluorimeter. The fluorescence quantum yield on PF108-R was determined by using Rhodamine 6G dissolved in EtOH as the reference standard (Φ_{ref} = 0.94). The absorption spectra were recorded on a Thermo Nicolet Evolution 300 spectrophotometer.

2.5. Cryogenic Transmission Electron Microscopy (cryo-TEM). Vitrified specimens were prepared in a controlled environment vitrification system (CEVS) at 25 °C and 100% relative humidity. A drop (~3 μL) of the sample was placed on a perforated carbon film-coated copper grid, blotted with filter paper, and plunged into liquid ethane at its freezing point. The vitrified specimens were transferred to a 626 Gatan cryo-holder and observed at 120 kV acceleration voltage in an FEI Tecnai T12 G^2 transmission electron microscope at about −175 °C in the low-dose imaging mode to minimize electron-beam radiation damage. Images were digitally recorded with a Gatan US1000 high-resolution CCD camera.

2.6. Small-Angle X-ray Scattering (SAXS). The characterization of the nanoparticle structure as a function of temperature was carried out by SAXS using a Ganesha 300XL (SAXSLAB ApS, Skovlunde, Denmark). This instrument is equipped with a 2D 300 K Pilatus detector (Dectris Ltd., Baden, Switzerland) and a Genix 3D X-ray source (Xenocs SA, Sassenage, France), generating X-rays at a wavelength, λ, of 1.54 Å. The scattering data was collected over a q range of $0.014 < q$ (Å^{-1}) < 0.753, where the magnitude of the scattering vector, q, is defined as $q = (4\pi/\lambda)\sin(\theta/2)$, where θ is the scattering angle. The two-dimensional scattering pattern was radially averaged using SAXSGui software to obtain $I(q)$. Measurements were performed in 1.5 mm quartz capillaries (Hilgenberg GmbH, Malsfeld, Germany). The temperature was controlled by an external recirculating water bath within ±0.3 °C. Samples were equilibrated for 1 h at the measurement temperature prior to performing the experiment.

DOI: 10.1021/acs.langmuir.5b02101
Langmuir 2015, 31, 9566−9575

Water channel radii of the reverse bicontinuous cubic phases were calculated using the relation $r_w = [(A_0/-2\pi\chi)^{1/2}a] - L$, where L is the length of the lipid hydrophobic chain (17 Å, in the case of MO), a is the lattice parameter obtained from the SAXS analysis, and A_0 and χ are the surface area and the Euler characteristic (integral Gaussian curvature scaled by 2π) of the infinite periodic minimal surface geometries within the unit cell, explained further in the Appendix ($Pn\underline{3}m$, $A_0 = 1.919$, $\chi = -2$; $Im\underline{3}m$, $A_0 = 2.345$, $\chi = -4$). At least two Bragg peaks were used to estimate the errors associated with a and r_w, unless otherwise indicated.

2.7. Light Scattering. Dynamic light scattering (DLS) experiments were performed to obtain the size evolution of the nanoparticles as a function of temperature. For that we used a light-scattering goniometer instrument (3D LS spectrometer, LS Instruments, Fribourg, Switzerland), equipped with a 35 mW He−Ne laser light source (wavelength of 632.8 nm). The instrument implements the so-called cross-correlation scheme to suppress contributions from multiple scattering[32−34] together with a modulation unit.[35] The samples were placed in 10 mm diameter cylindrical borosilicate disposable culture tubes (Fisherbrand, Thermo Fisher Scientific Inc., Waltham, MA, USA) and kept at the measurement temperature in a temperature-controlled index-matching bath. Samples were equilibrated at the measurement temperature for 10 min before the experiment. Measurements were performed at a range of scattering angles between 40 and 100° (in triplicate at each scattering angle). The initial decay rate, Γ, was derived from the second-order cumulant analysis of the normalized field autocorrelation function, which was used to calculate the apparent collective diffusion coefficient, D_0, of the nanoparticles

$$\Gamma = D_0 q^2 \tag{1}$$

where q is the module of the scattering vector, $q = (4\pi n/\lambda)\sin(\theta/2)$, with n being the refractive index of the solvent, λ being the wavelength of the incoming laser light, and θ being the scattering angle. The hydrodynamic radius, R_h, was obtained by the Stokes−Einstein relation ($D_0 = k_B T/6\pi\eta R_h$), where k_B is the Boltzmann constant, T is the absolute temperature, and η is the viscosity of the solvent at temperature T.

2.8. Cell Culture. HeLa cells (ATCC collection) were grown in phenol-red-free Dulbecco's modified Eagle's medium (DMEM, Molecular Probes, USA) with a high glucose concentration, supplemented with 10% (v/v) fetal bovine serum, penicillin (100 U mL^{-1}), and streptomycin (100 $\mu g\ mL^{-1}$) (Invitrogen) in a 5% CO_2 incubator at 37 °C. Cells were seeded in 35 mm dishes; experiments were carried out 2 days after seeding, when cells reached 90% confluency. Liquid-crystalline nanoparticles were added to the cells at a concentration of 1:500 (2 μL in 1 mL of fresh medium) and incubated at 37 °C for 4 h. For live cell imaging, fresh serum-free medium was used to remove the extracellular particle suspension before the imaging session.

2.9. Fluorescence Microscopy. Light microscopy observations were made using a Zeiss (Axioskop) upright fluorescence microscope (Zeiss, Oberkochen, Germany) equipped with 10×, 20×, and 40×/0.75 NA water immersion objectives and an HBO 50 W L-2 mercury lamp (Osram, Berlin, Germany). Twelve-bit-deep images were acquired with a monochrome-cooled CCD camera (QICAM, Qimaging, Canada). For the observation of dye fluorescence, filters were ex 546 ± 6 nm and em 620 ± 60 nm. Digital images were obtained with Image Pro Plus software (Media Cybernetics, Silver Springs, MD, USA).

2.10. Cytotoxic Activity (MTT Assay). The cytotoxic effect of cubosome formulations was evaluated in HeLa cells by the MTT assay. HeLa cells were seeded in 24-well plates at a density of 3×10^4 cells/well in 500 μL of serum-containing media. Experiments were carried out 2 days after seeding when cells had reached 90% confluence. The different formulations were added to the cells at a concentration of 1:500 (2 μL in 1 mL of serum-free medium) and incubated at 37 °C for 4 h. The effect of Docetaxel 10 μM (specifically, 1 μL of a 10 mM solution of Docetaxel in DMSO was added to 1 mL of serum-free medium) on HeLa cell viability was also tested for comparison at the same incubation time. A 50 μL portion of MTT solution (3-(4,5-dimethylthiazol-2-yl)-2,5-diphenyltetrazolium bromide) (5 mg/mL in H_2O) was then added and left for 2 h at 37 °C. The medium was aspirated, 500 μL of DMSO was added to the wells, and color development was measured at 570 nm with an Infinite 200 automicroplate reader (Infinite 200, Tecan, Austria). The absorbance is proportional to the number of viable cells. All measurements were performed in quadruplicate and repeated at least three times. Results are shown as the percentage of cell viability in comparison with nontreated control cells. Data were expressed as a mean ± standard deviation (SD) of three independent experiments involving quadruplicate analyses for each sample.

2.11. Determination of MO and Docetaxel Content in Cubosomes. After loading with Docetaxel, the cubosome dispersion was purified from the nonencapsulated drug by dialysis: 2 mL was loaded into a dialysis tubing cellulose membrane (14 kDa MW cutoff) and dialyzed against water (1000 mL) for 2 h (by replacing the water after 1 h) at 25 °C. It should be noticed that this purification step did not influence the concentration of the dye in the formulation since the fluorophore-conjugated PF108 has a MW higher than the membrane cutoff (about 16 kDa). Therefore, in comparison to traditional methods that require enclosing the dye within the lipid bilayer, this new procedure allows a huge saving of the (typically very expensive) dye. Aliquots (10 μL) of the nanoparticle preparations were dissolved in 300 μL of CH_3CN with 0.14% CH_3COOH (v/v). The samples were vortex mixed to obtain a clear solution, and aliquots (20 μL) were injected into the Agilent Technologies 1100 liquid chromatograph (Agilent Technologies, Palo Alto, CA) equipped with a diode array detector (DAD). Analyses of MO (detected at 200 nm) and Docetaxel (at 230 nm) in nanoparticle dispersions were carried out with a XDB−C_{18} Eclipse (150 × 4.6 mm^2, 3.5 mm particle size) (Agilent Technologies) equipped with a Zorbax XDB−C_{18} Eclipse (12.5 × 4.6 mm^2, 5 mm particle size) guard column (Agilent Technologies), with a mobile phase of $CH_3CN/H_2O/CH_3COOH$ (75/25/0.12 v/v/v) at a flow rate of 2.3 mL/min. The temperature of the column was maintained at 37 °C. Recording and integration of the chromatogram data was carried out through an Agilent OpenLAB chromatography data system. The identification of lipid components and drug was made using standard compounds and conventional UV spectra. Calibration curves of all of the compounds were constructed using standards and were found to be linear, with correlation coefficients >0.995.

The drug encapsulation efficacy (EE%) was calculated by the following equation:[36] EE% = (weight of the drug in nanoparticles)/(weight of the feeding drug) × 100%. Data were expressed as a mean ± standard deviation (SD) of three independent experiments involving duplicate analyses for each sample.

2.12. Statistical Analysis. An evaluation of the statistical significance of differences was performed using Graph Pad INSTAT software (GraphPad software, San Diego, CA, USA). Comparison between groups was assessed by one-way analysis of variance (one-way ANOVA) followed by the Bonferroni multiple comparisons test.

3. RESULTS

3.1. Synthesis of Rhodamine-Conjugated PF108 and Liquid-Crystalline Nanoparticle Characterization. When designing a nanoparticle for diagnostic or theranostic applications, two different approaches could be adopted: one is doping the nanoparticle with the imaging agent (a fluorescent probe, for instance); the other is functionalizing the nanoparticle with the imaging agent. This approach is quite straightforward in the case of silica-based nanoparticles, which can be easily functionalized by well-established siloxane chemistry.[37] The functionalization of nanoparticles as the cubosomes reported here can efficiently be achieved by conjugating the amphiphilic polymers used to stabilize the formulation (Pluronic F108, PF108, in our case) with a suitably

DOI: 10.1021/acs.langmuir.5b02101
Langmuir 2015, 31, 9566−9575

Scheme 1. Synthesis Procedure Adopted for the Preparation of PF108-R

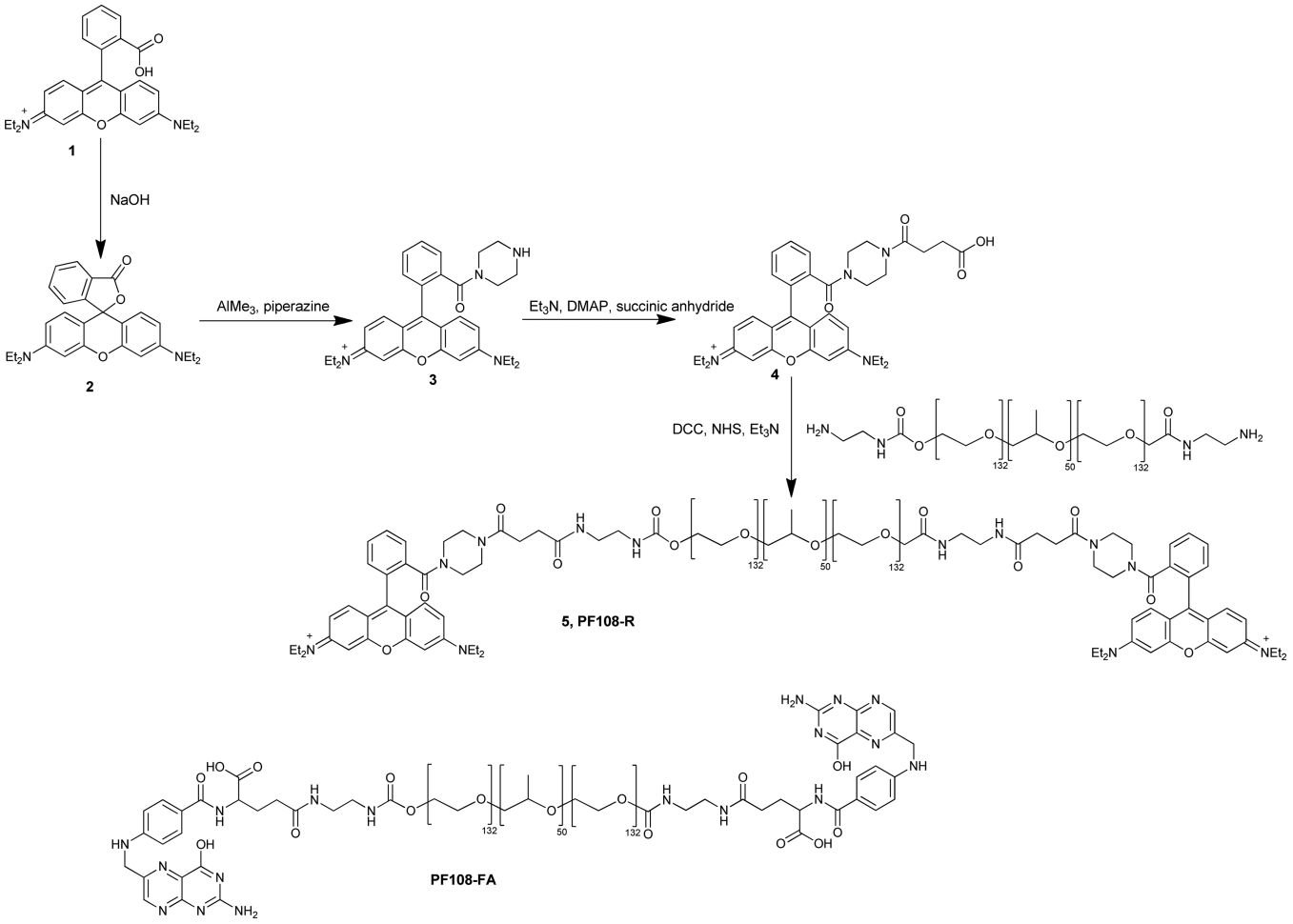

chemically modified imaging agent.[38] Here, fluorogenic molecule rhodamine B was conjugated to PF108 via a multisteps approach (Scheme 1). First, the fluorophore was synthetically modified as reported in the literature[39] to obtain its piperazine amide derivative (**4**) that was subsequently conjugated to the aminated derivative of PF108.[40] The reaction was carried out in DMSO in the presence of DCC, NHS, and Et_3N. Then, the product was dialyzed against deionized water and lyophilized.

Since the folate receptor is overexpressed on the cancer cell membrane, PF108 was also conjugated with folic acid as previously reported[20] to actively target the nanoparticles toward cancer tissues.

A mixture of commercial PF108, folate-conjugated PF108 (PF108-FA), and rhodamine-conjugated PF108 (PF108-R) was used to formulate cubosome dispersions in water also loaded with anticancer drug Docetaxel (DTX). According to preliminary tests, it was found that a mixture having the ratio PF108/PF108-FA/PF108-R = 60/20/20 (wt %) suitably stabilizes the dispersion for more than two months. This formulation was then investigated for its morphological and structural aspects by cryo-TEM, SAXS, and DLS measurements.

Figure 1 shows a typical cryo-TEM image of the cubosome formulation we proposed. A close inspection of the image in Figure 1 reveals a number of spherical cubosomes of different sizes and an inner structure characterized by a dark matrix and

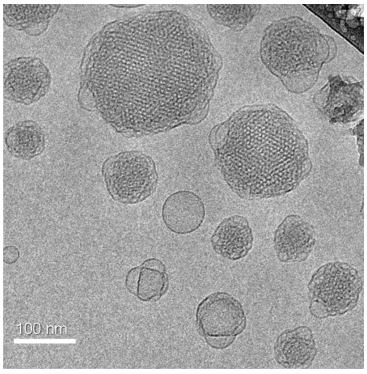

Figure 1. Cryo-TEM image of the cubosome formulation stabilized by a 60/20/20 mixture of commercial PF108, folate-conjugated PF108, and rhodamine-conjugated PF108.

alternate bright spots, respectively, representing the lipid bilayer and the water channels. As often occurs, some vesicular materials can be seen to be attached to the liquid-crystalline nanoparticles while, differently from other cubosome formulations, only a few vesicles are noticed. Indeed, unilamellar or oligolamellar vesicles typically form during the process of cubosome production, very likely because of the presence of the Pluronic used as a dispersant (MO in water does not produce small unilamellar or oligolamellar vesicles).[41] Actually, depending on the method of preparation, vesicles may exceed

DOI: 10.1021/acs.langmuir.5b02101
Langmuir 2015, 31, 9566−9575

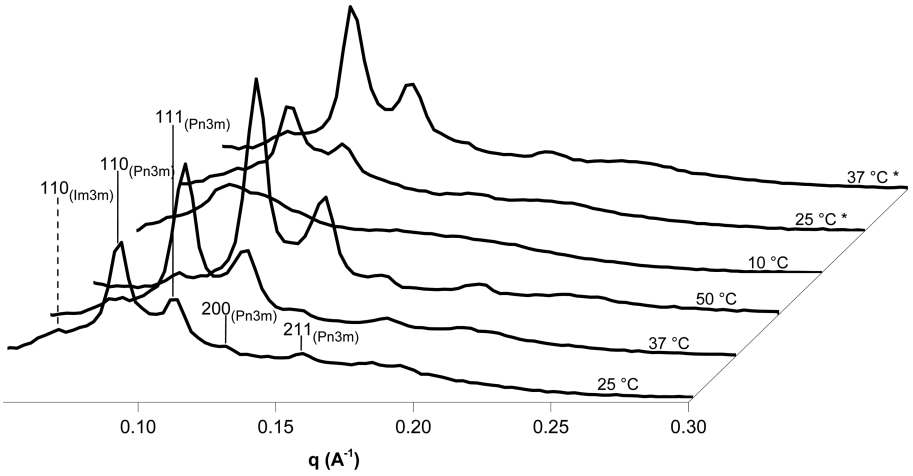

Figure 2. $I(q)$ vs q data obtained by SAXS recorded at different temperatures of the cubosome formulation stabilized by the same Pluronic mixture as in Figure 1. The Miller indices are reported on top of the corresponding Bragg peaks with the indication of the space group in the case of the bicontinuous cubic phases.

cubosomes in terms of number density.[42] Therefore, the absence of vesicular material observed here could be ascribed to the use of the conjugated Pluronics as a stabilizer for cubosome formulation.

Taking into account the possible use of the system under study as a theranostic nanocarrier, the variation of the size and inner structure upon temperature changes was monitored through DLS and SAXS measurements in the range of 10−50 °C. In particular, the temperatures were chosen to include two extreme storage temperatures (10 and 50 °C) as well as room and physiological temperatures. Moreover, to find out if the system nanostructure after temperature cycling is reestablished, SAXS measurements were performed in the following order: 25, 37, 50, 10, 25, and 37 °C. Results are reported in Figure 2 and Table 1.

Table 1. Cubosome Lattice Parameters (a) and Radius of the Water Channels (r_w)[a]

	$Pn\underline{3}m$		$Im\underline{3}m$[b]	
T (°C)	a (Å)	r_w (Å)	a (Å)	r_w (Å)
25	97.0 ± 0.5	20.9 ± 0.2	129.6	22.6
37	89.2 ± 0.2	17.9 ± 0.1	118.7	19.3
50	80.7 ± 0.2	14.5 ± 0.1	109.6	16.5
25	97.1 ± 0.6	21.2 ± 0.3	123.1	20.6
37	90.5 ± 0.7	18.4 ± 0.3	118.7	19.3

[a]Experiments were performed at different temperatures in the order reported in the table. [b]Standard deviations on a and r_w pertaining to $Im\underline{3}m$ phase were not reported since these parameters were obtained from the single Bragg peak discernible in the diffraction pattern.

SAXS results confirmed the bicontinuous cubic inner structure of the formulation. Actually, the diffraction pattern of the cubosome formulation at 25 °C (Figure 2) is dominated by four Bragg peaks placed in a q ratio of $2^{1/2}$:$3^{1/2}$:2:$6^{1/2}$ that clearly identify the double diamond ($Pn\underline{3}m$) bicontinuous cubic phase. However, a weak reflection at low q reveals the simultaneous presence of the primitive ($Im\underline{3}m$) bicontinuous cubic phase. The coexistence of the $Pn\underline{3}m$ and the $Im\underline{3}m$ phases in cubosome formulations is widely reported in the literature; it is attributed to a $Pn\underline{3}m$ to $Im\underline{3}m$ intercubic phase transition caused by the interaction of the hydrophobic moiety of the Pluronic with the surface of the cubosome nanoparticles.[43]

The lattice parameter, a, obtained from the SAXS experiments performed at different temperatures along with the calculated radius of the water channels r_w (section 2.3) are reported in Table 1. As usually detected in liquid-crystalline systems, although the nanostructure is retained, the lattice parameter (and consequently the radius of the water channels) of the cubosomes decreases while the temperature increases in the sequence 25, 37, 50 °C. This phenomenon is related to the enhanced disorder of the lipid chain at higher temperatures that, in turn, induces higher negative curvature at the lipid/water interface.[43] The disappearance of the weaker Bragg peaks detected in the diffraction patterns obtained at 10 °C (Figure 2) indicates that the inner structure is in some way altered, although not completely lost. When the temperature is raised again to 25 or 37 °C, the nanostructure is recovered. However, some significant differences can be noticed in the intensity of the Bragg peaks and the general appearance of the diffractograms after the temperature cycle. Therefore, it can be concluded that while the nanostructure is reestablished, the system evolution upon temperature changes is characterized by a certain degree of hysteresis.

The overall trend described by the DLS measurements of the nanoparticles' hydrodynamic radius can be extrapolated from the results reported in Table 2. Essentially, the nanoparticle average size does not vary significantly with temperature changes.

3.2. Rhodamine-Conjugated Liquid-Crystalline Nanoparticle Photophysical Characterization and HeLa Cell Imaging. The photophysical properties of PF108-R and those of cubosomes were investigated. Rhodamine dyes belong to the

Table 2. Average Hydrodynamic Radius (R_h) and Polydispersity Index (PdI) of the Cubosome Formulation at Different Temperatures

T (°C)	R_h (nm)	PdI
10	85	0.13
25	90	0.16
37	88	0.14
50	87	0.21

DOI: 10.1021/acs.langmuir.5b02101
Langmuir 2015, 31, 9566−9575

class of xanthene dyes, characterized by an intense red fluorescence, high brightness, excellent photostability, and the ability to modulate the properties of the dye through substitution.[44] A key property of these dyes is the equilibrium between an open, colored, fluorescent quinoid form or a closed, colorless, nonfluorescent lactone, which can be controlled by appropriate substitution.[45] In particular, rhodamine B (bearing two diethyl amino substituents) is one of the most common derivatives.

The emission/absorption properties of PF108-R were investigated in water and chloroform to test its photophysical features in media of different polarities. In both solvents PF108-R has a strong absorption band at 560 nm (ε = 30 660 M^{-1} cm^{-1}, 31 770 M^{-1} cm^{-1} in water and chloroform, respectively) and a shoulder at 522 nm (ε = 13 100 M^{-1} cm^{-1}, 9950 M^{-1} cm^{-1} in water and chloroform, respectively). Upon excitation at 522 nm in water, an emission band at 594 nm is generated. Conversely, the excitation at the same wavelength in chloroform generates a strong emission band at 584 nm. The quantum yields measured were 0.16 and 0.58, respectively, in water and chloroform. As expected, water has a quenching effect on the rhodamine fluorescence. The shift of the emission to higher energy could be explained by considering the solvatochromic properties of the fluorophore.

The emission spectrum of the cubosome formulation stabilized with the PF108/PF108-FA/PF108-R = 60/20/20 (wt %) mixture was also recorded after 1:100 dilution in water. Excitation at 522 nm resulted in emission bands centered at 581 nm (Figure 3). The position of the maximum emission

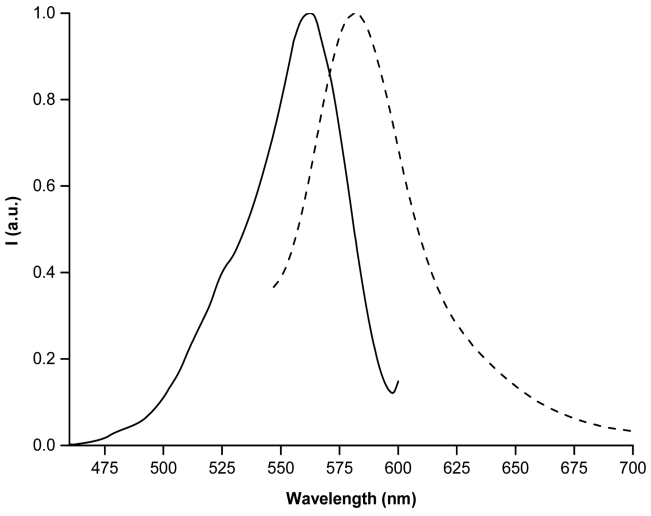

Figure 3. Normalized emission (λ_{exc} = 522 nm) and excitation (λ_{em} = 581 nm) spectra of the aqueous cubosome formulation stabilized using the same Pluronic mixture as in Figure 1.

wavelength is similar to that observed for PF108-R in chloroform. These results suggest that the rhodamine fragment conjugated to the Pluronic F108, rather than protruding toward the bulk water, is hidden within the poly(ethylene oxide) corona surrounding the nanoparticle, thus experiencing a less polar environment. The excitation spectrum of cubosomes is in accordance with PF108-R absorption in both water and chloroform. Due to the turbidity of the solution the determination of the quantum yield of the dye in the nanoparticles was not possible.

The uptake of cubosome nanoparticles was investigated by fluorescence microscopy. After 4 h of incubation, faint diffuse fluorescence was distributed within the cytoplasm of HeLa cells, whereas in untreated control cells no fluorescence was detected (Figure 4). However, it was not possible to determine whether the dye molecules were localized in specific cell compartments.

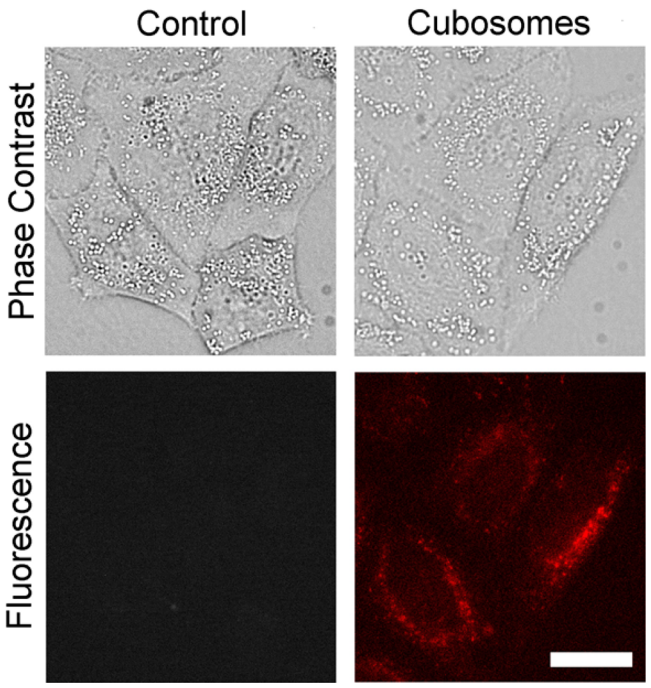

Figure 4. Fluorescence microscopy of living HeLa cells treated with cubosomes not carrying the drug (incubation for 4 h) showing a diffuse cytoplasmic fluorescence in treated cells indicating nanoparticle uptake. Scale bar = 20 μm.

3.3. Monoolein and Docetaxel Levels in Cubosome Formulations and Cytotoxic Activity (MTT Assay). The amount of MO (expressed as mg/mL of dispersion) and Docetaxel (DTX, μg/mL) in different cubosome formulations was monitored by HPLC. The formulations analyzed were the traditional cubosome formulation stabilized with PF108 (CUB), the cubosome formulation stabilized with the PF108/PF108-FA/PF108-R = 60/20/20 (wt %) mixture (CUB-R), and the latter formulation also loaded with DTX (CUB-R/DTX).

Monoolein contents in CUB, CUB-R, and CUB-R/DTX formulations were 33 ± 3, 35 ± 2, and 29 ± 2 mg/mL, respectively. The CUB-R/DTX formulation was loaded with 328 ± 25 μg/mL of drug, with a DTX/MO molecular ratio of 1/200. The encapsulation efficacy (EE%) was 103 ± 13%.

These formulations were tested for cytotoxicity (MTT assay) in HeLa cells. Figure 5 shows the viability, expressed as the % of the control, induced in HeLa cancer cells in the presence of the nanoparticle formulations at a concentration of 1:500 (2 μL/mL of medium) after 4 h of incubation. The cytotoxic effect of 10 μM DTX (section 2.10) was also determined after 4 h of incubation for comparison. Treatment with CUB and CUB-R formulations did not induce a significant reduction in cell viability, in comparison with control cells (Ctrl). Differently, the incubation with CUB-R/DTX particles induced a statistically significant decrease in HeLa cell viability (36% reduction)

DOI: 10.1021/acs.langmuir.5b02101
Langmuir 2015, 31, 9566−9575

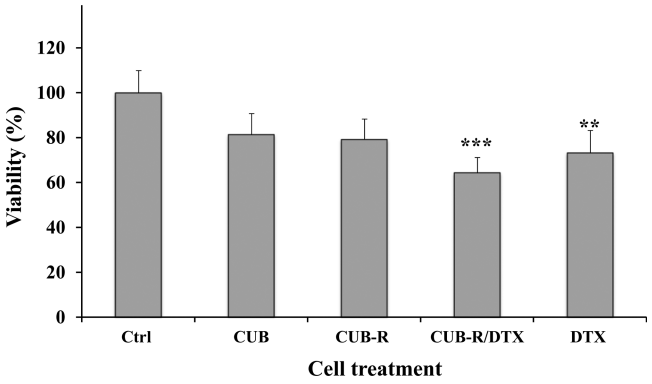

Figure 5. Viability, expressed as % of the control, induced in HeLa cells by incubation for 4 h in the presence of different types of cubosome formulations (CUB, CUB-R, and CUB-R/DTX, see the text) and Docetaxel (DTX). The drug concentration in the CUB-R/DTX formulation (0.8 μM) is 12.5-fold lower than in the DTX molecular dispersion (10 μM). Results are expressed as a mean ± standard deviation (SD) of four independent experiments involving quadruplicate analyses for each sample (n = 4). *** = P < 0.001; ** = P < 0.01 versus Ctrl, and data were analyzed using one-way ANOVA.

with respect to the control as a result of the presence of the anticancer drug. A significant cytotoxic effect (27% reduction in cell viability) was also observed in cells treated with the anticancer drug (DTX) directly added to the cell culture. Remarkably, the HeLa cell treatment with DTX-loaded cubosomes (DTX dose of approximately 0.8 μM) induced a superior cytotoxic effect compared to the molecularly dispersed anticancer drug tested at much higher (12.5-fold) concentration.

DTX is one of the most effective anticancer agents and has activity against a wide range of cancers. The growth inhibitory effect of DTX was examined in several cancer cell lines, and the IC_{50} (50% inhibitory concentration) values of this taxoid were in the nanomolar range at long-time incubation (72 h)[46,47] The 24 and 48 h IC_{50} values of the free DTX in HeLa cells were previously found to be 5.01 and 2.62 μg/mL, respectively.[48] Here, the higher cytotoxicity after 4 h of incubation of DTX administered via the nanoparticles (0.66 μg/mL) with respect to free drug molecules (8.08 μg/mL) can be explained by calling into play different uptake mechanisms. Indeed, cubosomes can deliver DTX into cells via endocytosis while free DTX can enter cells via passive diffusion with inherent lipophilicity, and various ABC efflux transporters, expressed at the cellular membrane, can minimize its effective penetration by efficiently eliminating the drug from the cell.[49]

3.4. Cubosomes versus Multilamellar Liposome Hydrophobic Volume. One important feature that distinguishes cubosomes (reverse bicontinuous cubic liquid-crystalline nanoparticles) from liposomes (their lamellar counterpart) is the higher hydrophobic volume of the former. Since cubosomes are mainly proposed as nanocarriers for hydrophobic molecules of pharmaceutical interest as an alternative to liposomes, this fact may be extremely relevant in view of their theranostic applications. Given the very convoluted volumes occupied by lipid chains in bicontinuous morphologies compared to the shells of liposomes, it is tempting to assume that the former contains a far larger hydrophobic volume (suitably) normalized than the latter. Surprisingly, the quantification of the hydrophobic volumes of bicontinuous cubosomes with respect to multilamellar liposomes has never been reported.

Assume for simplicity that we have two nanoparticles composed of monoolein in water whose outer diameter is 100 nm. Assume that the liposome is composed of N concentric spherical monoolein bilayers, composed of pairs of monolayers, each with a hydrophobic thickness of 17 Å, corresponding to the likely chain length in molten monoolein assemblies. Furthermore, assume that adjacent bilayers are separated by polar films that are 16 Å thick, so that each monolayer has an associated polar layer of thickness of 8 Å (corresponding to dimensions in the fully hydrated lamellar mesophase).[50] Each repeat unit of chains, monoolein headgroups, and water is therefore 50 Å thick. The hydrophobic volume is then calculated as the chain contribution to the total volume within N concentric nested shells whose outermost radius is scaled such that the outermost monolayer and associated polar layer has a diameter of 100 nm. These dimensions imply that the hydrophobic volume fractions within the liposome (whose total volume is 5.24×10^5 nm^3) are approximately 0.18, 0.33, 0.445, 0.53, and 0.59 nm^3 for N = 1−5 bilayers, respectively. The exposed outermost monolayer has an area of 2.83×10^4 nm^2.

The structural dimensions of a typical cubosome can be estimated as follows. We assume the cubosome to be a single-crystalline domain of the $Im\underline{3}m$ phase, also contained within a spherical shell of diameter 100 nm (cubosome nanoparticles, although characterized by a cubic inner nanostructure, can be spherical in shape, such as those shown in Figure 1). We choose a typical lattice dimension of the $Im\underline{3}m$ unit cell, namely, 130 Å, and fix the chain length to be the same as that in the liposome, 17 Å (the polar dimensions are then fixed by those parameters). The resulting total exposed area is then 1.68×10^5 nm^2 (equal to the summed area of each monolayer displaced 17 Å from the bilayer midsurface, whose geometry is assumed to lie on the P surface, the cubic periodic $Im\underline{3}m$ minimal surface). Surprisingly, the membrane area exposed to water in the liposome is substantially larger than the total area in the cubosome. The corresponding hydrophobic volume fraction within the 100 nm cubosomal sphere is 0.59 nm^3, which is greater than that of the liposome with up to five bilayers (Table 3).

Table 3. Cubosome-to-Liposome Hydrophobic Volume Ratios (V_h) as a Function of the Number of Concentric Bilayers in the Liposome[a]

number of bilayers	1	2	3	4	5
V_h ratios	3.22	1.79	1.33	1.12	1.00

[a]See also the text.

4. CONCLUSIONS

In this paper we demonstrated that cubosomes loaded with an anticancer drug, namely, Docetaxel, can be formulated by decorating their nanoparticle surface with both a cancer-cell-targeting ligand and an imaging probe. It is worth noticing that this is the first time that Docetaxel is successfully loaded within cubosomes and that the cubosome surface is simultaneously decorated with targeting and imaging moieties. To this aim, the commercial block copolymer Pluronic F108 (PF108) and its folate- and rhodamine-conjugated counterparts were used in a 60/20/20 (wt %) mixture to stabilize the lipid liquid-crystalline

DOI: 10.1021/acs.langmuir.5b02101
Langmuir 2015, 31, 9566−9575

dispersion. SAXS, DLS, and cryo-TEM investigation, over the temperatures range explored, confirmed the cubic bicontinuous inner structure of the nanoparticles and showed the physicochemical aspects (morphology and size) akin to those of traditionally prepared cubosome dispersions. Photophysical measurements suggested that the fluorogenic fragment, although conjugated to the terminal ethylenoxide moiety of PF108, was very likely exposed to the less polar environment constituted by the poly(ethylene oxide) corona surrounding the nanoparticles, rather than protruding toward the bulk water. This formulation, not loaded with the drug, was successfully used to image living HeLa cells. Besides, viability tests revealed a significant cytotoxic effect (more than 1 order of magnitude larger than the molecularly dispersed drug) of the Docetaxel-loaded nanoparticles against HeLa cells. These results evidenced that the loading of cubosomes with a Docetaxel dose able to induce cytotoxic effects on HeLa cells and the decoration of their surface with 40% conjugated PF108 did not compromise the intrinsic nature of these peculiar nanoparticles and their cellular uptake. We have also evaluated the differences between cubosomes and multilamellar liposomes in terms of surface area and hydrophobic volume. Under the imposed constraints (same molecular building block and nanoparticle volume, cubosome nanostructure characterized by the $Im\bar{3}m$ space group with a lattice parameter of 130 Å, and multilamellar liposome constituted of adjacent bilayers), these calculations demonstrated that the hydrophobic volume of cubosomes is more than 3 times larger than that of single-bilayer liposomes, but the cubosome-to-liposome hydrophobic volume ratio rapidly converges to unity as the number of the bilayers in the liposome increases. It is worth noting that this ratio will be even larger if the liposome contains nonadjacent bilayers. Remarkably, the cubosome surface exposed to water is about 60% with respect to that of the liposome.

Taken together, these findings demonstrate the good performance of cubosomes as peculiar nanocarriers for hydrophobic molecules with therapeutic/diagnostic relevance and encourage the investigation of a cubic bicontinuous liquid-crystalline dispersion for possible applications as theranostic tools.

APPENDIX

Geometrical Calculations

Denote the chain length by d, the thickness of the polar layer (containing water plus headgroups) by t, and the lattice parameter in the cubic mesophase by a. Assume that the outer shape of the liposome and the cubosome is a sphere of outer diameter L.

We assume that all interfaces, lining the monolayers at the chain−water interface and the free chain ends, are parallel. We then use the formalism described elsewhere[1] to deduce dimensions. All dimensions are calculated from the geometry of the imaginary surface S that runs between the chain ends in opposed monolayers at the midsection of the hydrophobic shell for each bilayer. The "outer" surfaces, exposed to water, are parallel to S and displaced by d from S. We have two formulae derived from the geometry of parallel surfaces, both related to the mean and Gaussian curvatures of S, denoted H_S and K_S, respectively. One is for the area of the surface Sx, parallel to S, displaced by a distance x

$$\text{area}(Sx) = \text{area}(S)(1 + 2Hx + Kx^2)$$

(where the sign of x depends on whether it is on the outside or the inside of the surface). The second describes the volume of the film lying in between S and Sx:

$$\text{volume}(Sx) = \text{area}(S)x\left(1 + Hx + \frac{Kx^2}{3}\right)$$

In the liposome, those surfaces are parallel spheres, and if it is made of N bilayers, there are N such spheres, each one with radius

$$r(i) = \frac{L}{2} - (2i - 1)(d + t)$$

These dimensions impose mean and Gaussian curvatures on bilayer i equal to

$$H(i) = r(i)^{-1}$$

$$K(i) = r(i)^{-2}$$

The exposed area of the liposome is that of the outermost spherical monolayer (displaced a distance t inwards from the 100 nm external shell), namely, $4\pi r(1)^2$. The total volume is $V_{\text{total}} = (4/3)\pi(L/2)^3$. The hydrophobic (chain) volume in the liposome is determined by summing over all $2N$ monolayers, N displaced x and N displaced $-x$:

$$\text{volume}(N) = 4\pi d \sum_{i=1}^{N} r(i)^2 \left\{\left(1 + H(i)d + \frac{d^2}{3K(i)}\right) + \left(1 - H(i)d + \frac{d^2}{3K(i)}\right)\right\} \quad (1)$$

The corresponding calculation for the cubosome follows directly from the normalized surface to volume ratio or "homogeneity index" characteristic of a particular folded surface geometry

$$\mathcal{H}: = \frac{\text{area}_Q{}^{3/2}}{(-2\pi\chi)^{1/2}\text{volume}}$$

where χ is the Euler characteristic of the hyperbolic bilayer within the particle. If the cubosome is contained within a spherical shell of diameter L and the membrane within folds onto a periodic minimal surface to form a cubic lattice of edge a whose topology per unit cell is χ_0, then $\chi = \chi_0(V_{\text{total}}/\alpha^3)$. The radius of curvature of the minimal surface is given by the expression

$$r_Q = \left\{\frac{\mathcal{H}}{-2\pi\chi}\right\}^{1/3}$$

which corresponds to minimal surface curvatures $H_Q = 0$ and $K_Q = -r_Q{}^{-2}$.[50] It follows that the minimal surface area in the cubosome is

$$\text{area}_Q = \{\mathcal{H}V_{\text{total}}(-2\pi\chi)^{1/2}\}^{2/3}$$

so that the exposed area (at the hydrophobic/hydrophilic interface) is

$$\text{area}_{\text{exposed}} = 2\text{area}_Q(1 - Kd^2)$$

and the hydrophobic volume is

DOI: 10.1021/acs.langmuir.5b02101
Langmuir 2015, 31, 9566−9575

$$\text{volume}_{Q} = 2\text{area}_{\text{exposed}}\left(1 + \frac{d^3}{3K_Q}\right) \quad (2)$$

If the internal bilayer geometry within the cubosome corresponds to the *Im3m* bicontinuous mesophase, then the relevant data are $\mathcal{H} = 0.7163$ and $\chi_0 = -4$.[51] The ratios of hydrophobic volumes are calculated from the results of eqs 1 and 2 above.

AUTHOR INFORMATION

Corresponding Authors

*E-mail: ccaltagirone@unica.it. Tel: +39(0)70 675 4453.
*E-mail: murgias@unica.it. Tel: +39(0)70 675 4453.

Notes

The authors declare no competing financial interest.

ACKNOWLEDGMENTS

Karin Schillén and Tommy Nylander are kindly thanked for fruitful discussions. We acknowledge financial support from the European Commission under the Seventh Framework Program by means of the grant agreement for the Integrated Infrastructure Initiative (no. 262348) European Soft Matter Infrastructure (ESMI). Financial support by MIUR (project PRIN 2010BJ23MN_002), Fondazione Banco di Sardegna, and Regione Autonoma della Sardegna (CRP-59699) is gratefully acknowledged. Sardegna Ricerche Scientific Park (Pula, CA, Italy) is acknowledged for free access to the facilities of the Nanobiotechnology Laboratory. The cryo-TEM work was performed at the Technion Laboratory for Electron Microscopy of Soft Matter, supported by the Technion Russell Berrie Nanotechnology Institute (RBNI).

REFERENCES

(1) Hyde, S.; Andersson, S.; Larsson, K.; Blum, Z.; Landh, T.; Lidin, S.; Ninham, B. W. *The Language of Shape*; Elsevier: Amsterdam, 1997; Chapters 1−5.

(2) Luzzati, V.; Husson, F. The structure of the liquid-crystalline phases of lipid−water systems. *J. Cell Biol.* **1962**, *12*, 207−219.

(3) Larsson, K. Cubic lipid-water phases: Structure and biomembrane aspects. *J. Phys. Chem.* **1989**, *93*, 7304−7314.

(4) Bender, J.; Ericson, M. B.; Merclin, N.; Iani, V.; Rosén, A.; Engström, S.; Moan, J. Lipid cubic phases for improved topical drug delivery in photodynamic therapy. *J. Controlled Release* **2005**, *106*, 350−360.

(5) Caboi, F.; Amico, G. S.; Pitzalis, P.; Monduzzi, M.; Nylander, T.; Larsson, K. Addition of hydrophilic and lipophilic compounds of biological relevance to the monoolein/water system. I. Phase behavior. *Chem. Phys. Lipids* **2001**, *109*, 47−62 and references therein..

(6) Lopes, L. B.; Collett, J. H.; Bentley, M. V. L. B. Topical delivery of cyclosporin A: an in vitro study using monoolein as a penetration enhancer. *Eur. J. Pharm. Biopharm.* **2005**, *60*, 25−30.

(7) Monduzzi, M.; Lampis, S.; Murgia, S.; Salis, A. From self-assembly fundamental knowledge to nanomedicine developments. *Adv. Colloid Interface Sci.* **2014**, *205*, 48−67.

(8) Murgia, S.; Caboi, F.; Monduzzi, M. Addition of hydrophilic and lipophilic compounds of biological relevance to the monoolein/water system II — 13C NMR relaxation study. *Chem. Phys. Lipids* **2001**, *110*, 11−17.

(9) Mulet, X.; Boyd, B. J.; Drummond, C. J. Advances in drug delivery and medical imaging using colloidal lyotropic liquid crystalline dispersions. *J. Colloid Interface Sci.* **2013**, *393*, 1−20.

(10) Chong, J. Y. T.; Mulet, X.; Postma, A.; Keddie, D. J.; Waddington, L. J.; Boyd, B. J.; Drummond, C. J. Novel RAFT amphiphilic brush copolymer steric stabilisers for cubosomes: poly(octadecyl acrylate)- block-poly(polyethylene glycol methyl ether acrylate). *Soft Matter* **2014**, *10*, 6666−6676.

(11) Chong, J. Y. T.; Mulet, X.; Waddington, L. J.; Boyd, B. J.; Drummond, C. J. High-Throughput Discovery of Novel Steric Stabilizers for Cubic Lyotropic Liquid Crystal Nanoparticle Dispersions. *Langmuir* **2012**, *28*, 9223−9232.

(12) Johnsson, M.; Barauskas, J.; Norlin, A.; Tiberg, F. Physicochemical and drug delivery aspects of lipid-based liquid crystalline nanoparticles: a case study of intravenously administered propofol. *J. Nanosci. Nanotechnol.* **2006**, *6*, 3017−3024.

(13) Esposito, E.; Ravani, L.; Mariani, P.; Contadod, C.; Drechsler, M.; Puglia, C.; Cortesi, R. Curcumin containing monoolein aqueous dispersions: A preformulative study. *Mater. Sci. Eng., C* **2013**, *33*, 4923−4934.

(14) Fraser, S. J.; Rose, R.; Hattarki, M. K.; Hartley, P. G.; Dolezal, O.; Dawson, R. M.; Separovica, F.; Polyzos, A. Preparation and biological evaluation of self-assembled cubic phases for the polyvalent inhibition of cholera toxin. *Soft Matter* **2011**, *7*, 6125−6134.

(15) Montis, C.; Castroflorio, B.; Mendozza, M.; Salvatore, A.; Berti, D.; Baglioni, P. Magnetocubosomes for the delivery and controlled release of therapeutics. *J. Colloid Interface Sci.* **2015**, *449*, 317−326.

(16) Rattanapak, T.; Birchall, J.; Young, K.; Ishii, M.; Meglinski, I.; Rades, T.; Hook, S. Transcutaneous immunization using microneedles and cubosomes: Mechanistic investigations using Optical Coherence Tomography and Two-Photon Microscopy. *J. Controlled Release* **2013**, *172*, 894−903.

(17) Rizwan, S. B.; McBurney, W. T.; Young, K.; Hanley, T.; Boyd, B. J.; Rades, T.; Hook, S. Cubosomes containing the adjuvants imiquimod and monophosphoryl lipid A stimulate robust cellular and humoral immune responses. *J. Controlled Release* **2013**, *165*, 16−21.

(18) Gupta, A.; Stait-Gardner, T.; de Campo, L.; Waddington, L. J.; Kirby, N.; Price, W. S.; Moghaddam, M. J. Nanoassemblies of Gd−DTPA−monooleyl and glycerol monooleate amphiphiles as potential MRI contrast agents. *J. Mater. Chem. B* **2014**, *2*, 1225−1233.

(19) Moghaddam, M. J.; de Campo, L.; Hirabayashi, M.; Bean, P. A.; Waddington, L. J.; Scoble, J. A.; Coiac, G.; Drummond, C. J. Gadolinium-DTPA amphiphile nanoassemblies: agents for magnetic resonance imaging and neutron capture therapy. *Biomater. Sci.* **2014**, *2*, 924−935.

(20) Caltagirone, C.; Falchi, A. M.; Lampis, S.; Lippolis, V.; Meli, V.; Monduzzi, M.; Prodi, L.; Schmidt, J.; Sgarzi, M.; Talmon, Y.; Bizzarri, R.; Murgia, S. Cancer Cell-Targeted Theranostic Cubosomes. *Langmuir* **2014**, *30*, 6228−6236.

(21) Deshpande, S.; Venugopal, E.; Ramagiri, S.; Bellare, J. R.; Kumaraswamy, G.; Singh, N. Enhancing Cubosome Functionality by Coating with a Single Layer of Poly-ε-lysine. *ACS Appl. Mater. Interfaces* **2014**, *6*, 17126−17133.

(22) Muir, B. W.; Acharya, D. P.; Kennedy, D. F.; Mulet, X.; Evans, R. A.; Pereira, S. M.; Wark, L. K.; Boyd, B. J.; Nguyen, T.-H.; Hinton, T. M.; Waddington, J. L.; Kirby, N.; Wright, D. K.; Wang, H. X.; Egan, F. G.; Moffat, B. A. Metal-free and MRI visible theranostic lyotropic liquid crystal nitroxide-based nanoparticles. *Biomaterials* **2012**, *33*, 2723.

(23) Murgia, S.; Bonacchi, S.; Falchi, A. M.; Lampis, S.; Lippolis, V.; Meli, V.; Monduzzi, M.; Prodi, L.; Schmidt, J.; Talmon, Y.; Caltagirone, C. Drug Loaded Fluorescent Cubosomes: Versatile Nanoparticles for Potential Theranostic Applications. *Langmuir* **2013**, *29* (22), 6673−6679.

(24) Murgia, S.; Falchi, A. M.; Meli, V.; Schillén, K.; Lippolis, V.; Monduzzi, M.; Rosa, A.; Schmidt, J.; Talmon, Y.; Bizzarri, R.; Caltagirone, C. Cubosome formulations stabilized by a dansyl-conjugated block copolymer for possible nanomedicine applications. *Colloids Surf., B* **2015**, *129*, 87−94.

(25) Nilsson, C.; Barrios-Lopez, B.; Kallinen, A.; Laurinmäki, P.; Butcher, S. J.; Raki, M.; Weisell, J.; Bergström, K.; Larsen, S. W.; Østergaard, J.; Larsen, C.; Urtti, A.; Airaksinen, A. J.; Yaghmur, A. SPECT/CT imaging of radiolabeled cubosomes and hexosomes for potential theranostic applications. *Biomaterials* **2013**, *34*, 8491−8503.

DOI: 10.1021/acs.langmuir.5b02101
Langmuir 2015, 31, 9566−9575

(26) Barreto, J. A.; O'Malley, W.; Kubeil, M.; Graham, B.; Stephan, H.; Spiccia, L. Nanomaterials: applications in cancer imaging and therapy. *Adv. Mater.* **2011**, *23*, H18.
(27) Pombo García, K.; Zarschler, K.; Barbaro, L.; Barreto, J. A.; O'Malley, W.; Spiccia, L.; Stephan, H.; Graham, B. Zwitterionic-Coated "Stealth" Nanoparticles for Biomedical Applications: Recent Advances in Countering Biomolecular Corona Formation and Uptake by the Mononuclear Phagocyte System. *Small* **2014**, *10*, 2516−2529.
(28) Caltagirone, C.; Arca, M.; Falchi, A. M.; Lippolis, V.; Meli, V.; Monduzzi, M.; Nylander, T.; Rosa, A.; Schmidt, J.; Talmon, Y.; Murgia, S. Solvatochromic fluorescent BODIPY derivative as imaging agent in camptothecin loaded hexosomes for possible theranostic applications. *RSC Adv.* **2015**, *5*, 23443−23449.
(29) Zhai, J.; Scoble, J. A.; Li, N.; Lovrecz, G.; Waddington, L. J.; Tran, N.; Muir, B. W.; Coia, G.; Kirby, N.; Drummond, C. J.; Mulet, X. Epidermal growth factor receptor-targeted lipid nanoparticles retain self-assembled nanostructures and provide high specificity. *Nanoscale* **2015**, *7*, 2905−2913.
(30) Falchi, A. M.; Rosa, A.; Atzeri, A.; Incani, A.; Lampis, S.; Meli, V.; Caltagirone, C.; Murgia, S. Effects of monoolein-based cubosome formulations on lipid droplets and mitochondria of HeLa cells. *Toxicol. Res.* **2015**, *4*, 1025−1036.
(31) Janiak, J.; Bayati, S.; Galantini, L.; Pavel, N. V.; Schillén, K. Nanoparticles with a Bicontinuous Cubic Internal Structure Formed by Cationic and Non-ionic Surfactants and an Anionic Polyelectrolyte. *Langmuir* **2012**, *28*, 16536−16546.
(32) Phillies, G. D. J. Experimental Demonstration of Multiple-Scattering Suppression in Quasielastic-Light-Scattering Spectroscopy by Homodyne Coincidence Techniques. *Phys. Rev. A: At., Mol., Opt. Phys.* **1981**, *24*, 1939−1943.
(33) Schätzel, K. Suppression of Multiple Scattering by Photon Cross-correlation Techniques. *J. Mod. Opt.* **1991**, *38*, 1849−1865.
(34) Urban, C.; Schurtenberger, P. Characterization of Turbid Colloidal Suspensions Using Light Scattering Techniques Combined with Cross-Correlation Method. *J. Colloid Interface Sci.* **1998**, *207*, 150−158.
(35) Block, I. D.; Scheffold, F. Modulated 3D cross-correlation light scattering: Improving turbid sample characterization. *Rev. Sci. Instrum.* **2010**, *81*, 123107.
(36) Liu, Z.; Liu, D.; Wang, L.; Zhang, J.; Zhang, N. Docetaxel-Loaded Pluronic P123 Polymeric Micelles: in Vitro and in Vivo Evaluation. *Int. J. Mol. Sci.* **2011**, *12*, 1684−1696.
(37) Caltagirone, C.; Bettoschi, A.; Garau, A.; Montis, R. Silica-based nanoparticles: a versatile tool for the development of efficient imaging agents. *Chem. Soc. Rev.* **2015**, *44*, 4645.
(38) Breul, A. M.; Hager, M. D.; Schubert, U. S. Fluorescent monomers as building blocks for dye labeled polymers: synthesis and application in energy conversion, biolabeling and sensors. *Chem. Soc. Rev.* **2013**, *42*, 5366−5407.
(39) Nguyen, T.; Francis, M. B. Practical Synthetic Route to Functionalized Rhodamine Dyes. *Org. Lett.* **2003**, *5*, 3245−3248.
(40) Zhang, W.; Shi, Y.; Chen, Y.; Ye, J.; Sha, X.; Fang, X. Multifunctional Pluronic P123/F127 mixed polymeric micelles loaded with paclitaxel for the treatment of multidrug resistant tumors. *Biomaterials* **2011**, *32*, 2894−2906.
(41) Murgia, S.; Falchi, A. M.; Mano, M.; Lampis, S.; Angius, R.; Carnerup, A. M.; Schmidt, J.; Diaz, G.; Giacca, M.; Talmon, Y.; Monduzzi, M. Nanoparticles from lipid-based liquid crystals: emulsifier influence on morphology and cytotoxicity. *J. Phys. Chem. B* **2010**, *114* (10), 3518−3525.
(42) Barauskas, J.; Johnsson, M.; Joabsson, F.; Tiberg, F. Cubic Phase Nanoparticles (Cubosome†): Principles for Controlling Size, Structure, and Stability. *Langmuir* **2005**, *21*, 2569−2577.
(43) Nakano, M.; Sugita, A.; Matsuoka, H.; Handa, T. Small-Angle X-ray Scattering and 13C NMR Investigation on the Internal Structure of "Cubosomes. *Langmuir* **2001**, *17*, 3917−3922.
(44) Beija, M.; Afonso, C. A. M.; Martinho, J. M. G. Synthesis and applications of Rhodamine derivatives as fluorescent probes. *Chem. Soc. Rev.* **2009**, *38*, 2410−2433.
(45) Lavis, L. D.; Chao, T.-Y.; Raines, R. T. Fluorogenic Label for Biomolecular Imaging. *ACS Chem. Biol.* **2006**, *1*, 252−260.
(46) Domingo-Domenech, J.; Oliva, C.; Rovira, A.; Codony-Servat, J.; Bosch, M.; Filella, X.; Montagut, C.; Tapia, M.; Campás, C.; Dang, L.; Rolfe, M.; Ross, J. S.; Gascon, P.; Albanell, J.; Mellado, B. Interleukin 6, a nuclear factor-kappaB target, predicts resistance to docetaxel in hormone-independent prostate cancer and nuclear factor-kappaB inhibition by PS-1145 enhances docetaxel antitumor activity. *Clin. Cancer Res.* **2006**, *12*, 5578−86.
(47) Zhu, S.; Oremo, J. A.; Li, S.; Zhen, M.; Tang, Y.; Du, Y. Synergistic antitumor activities of docetaxel and octreotide associated with apoptotic-upregulation in castration-resistant prostate cancer. *PLoS One* **2014**, *9*, e91817.
(48) Zhu, H.; Chen, H.; Zeng, X.; Wang, Z.; Zhang, X.; Wu, Y.; Gao, Y.; Zhang, J.; Liu, K.; Liu, R.; Cai, L.; Mei, L.; Feng, S. S. Co-delivery of chemotherapeutic drugs with vitamin E TPGS by porous PLGA nanoparticles for enhanced chemotherapy against multi-drug resistance. *Biomaterials* **2014**, *35*, 2391−2400.
(49) Shen, H.; Lee, F. Y.; Gan, J. Ixabepilone, a novel microtubule-targeting agent for breast cancer, is a substrate for P-glycoprotein (P-gp/MDR1/ABCB1) but not breast cancer resistance protein (BCRP/ABCG2). *J. Pharmacol. Exp. Ther.* **2011**, *337*, 423−432.
(50) Chung, H.; Caffrey, M. The Neutral Area Surface of the Cubic Mesophase: Location and Properties. *Biophys. J.* **1994**, *66*, 377−381.
(51) Hyde, S. Bicontinuous structures in lyotropic liquid crystals and crystalline hyperbolic surfaces. *Curr. Opin. Solid State Mater. Sci.* **1996**, *1*, 653−662.

DOI: 10.1021/acs.langmuir.5b02101
Langmuir 2015, 31, 9566−9575